Raman signature of the non-hydrogen-bonded tryptophan side chain in proteins: Experimental and ab initio spectra of 3-methylindole in the gas phase

ARTICLE *in* JOURNAL OF MOLECULAR STRUCTURE · FEBRUARY 2005

Impact Factor: 1.6 · DOI: 10.1016/j.molstruc.2004.11.058

Available online at www.sciencedirect.com
SCIENCE DIRECT
Journal of Molecular Structure 735–736 (2005) 271–278
Journal of MOLECULAR STRUCTURE
www.elsevier.com/locate/molstruc

Raman signature of the non-hydrogen-bonded tryptophan side chain in proteins: experimental and ab initio spectra of 3-methylindole in the gas phase ☆

Amanda Combs[a], Kathleen McCann[a], Daniel Autrey[a,1], Jaan Laane[a,*], Stacy A. Overman[b], George J. Thomas Jr.[b,*]

[a]*Department of Chemistry, Texas A&M University, College Station, TX 77843-3255, USA*
[b]*School of Biological Sciences, University of Missouri-Kansas City, Kansas City, MO 64110-2499, USA*

Received 1 October 2004; revised 15 November 2004; accepted 17 November 2004

Abstract

3-Methylindole (3MI), which serves as a structural model for the tryptophan side chain in proteins, has been investigated using vapor phase Raman spectroscopy. The vapor phase spectrum of 3MI identifies the Raman signature of the indolyl moiety free of intermolecular interaction and extends previously reported solution Raman studies of 3MI and related tryptophan derivatives. The Raman spectrum of 3MI vapor is also complemented here with newly obtained vapor phase infrared data and ab initio calculations to refine and extend previous vibrational assignments. The present results provide an improved basis for assessing the dependence of the indolyl Raman signature on the local environment of the tryptophan side chain of proteins. The principal conclusions of this work are the following. (i) The vapor phase 3MI molecule exhibits Raman bands at 3506, 1585, 1409, 1349/1341 (Fermi doublet) and 881 cm^{-1}, which differ greatly from their counterparts in the Raman spectrum of 3MI liquid and thus serve as spectral markers of the indolyl ring environment. (ii) The Fermi doublet relative intensity ratio (I_1/I_2, where I_1 and I_2 are, respectively, the Raman intensities of the higher and lower wavenumber components of the doublet) is highly sensitive to the state of 3MI condensation, consistent with the previously reported sensitivity of I_1/I_2 to solvent polarity. The maximum value of the intensity ratio ($I_1/I_2=3.0$) is observed for 3MI vapor, while the minimum value ($I_1/I_2=0.43$) is observed for 3MI in $CHCl_3$ solution. Implications of the present results for Raman analysis of hydrogen bonding states, hydrophilic interactions and hydrophobic interactions of tryptophan residues in proteins are considered.

Keywords: Structure; Protein; Tryptophan; Hydrogen bonding; Raman spectroscopy; Vibrational spectra; Ab initio; 3-Methylindole

1. Introduction

The effectiveness of Raman spectroscopy as a protein structural probe relies upon accurate vibrational assignments for the many spectral bands contributed by both the main chain and diverse side chains of the protein. Also required are definitive correlations linking key parameters of the Raman bands, such as spectral frequency (wavenumber), relative intensity and polarization, to the local environments of the protein moieties to which the bands are assigned. Because the main-chain peptide moiety is the most prevalent chemical group in every protein, its Raman markers (so-called amide bands) are typically the most prominent in the spectra. Accordingly, the Raman amide bands have been investigated extensively and are the best understood in terms of quantitative relationships between their spectral attributes and the local environment or conformation of the protein main chain. Pre-eminent

Abbreviations: 3MI, 3-methylindole or skatole; Trp, tryptophan; Tyr, tyrosine; Cys, cysteine; Phe, phenylalanine; UVRR, ultraviolet-resonance Raman; ρ, Raman depolarization ratio.

☆ Part XC in the series Structural Studies of Viruses by Raman Spectroscopy.

* Corresponding authors. Fax: +1 816 235 1503 (G.J. Thomas) Fax: +1 979 845 3154 (J. Laane).

E-mail addresses: laane@mail.chem.tamu.edu (J. Laane), thomasgj@umkc.edu (G.J. Thomas).

[1] Present address: Department of Natural Sciences, Fayetteville State University, Fayetteville, NC 28301, USA.

0022-2860/$ - see front matter © 2004 Elsevier B.V. All rights reserved.
doi:10.1016/j.molstruc.2004.11.058

among Raman amide bands is the carbonyl-related amide I mode, which generally occurs within the 1640–1700 cm^{-1} interval of the Raman spectrum [1–4].

Also prominent in Raman spectra of proteins are bands assigned to skeletal stretching modes of electron-rich groups, including vibrations associated with the aromatic rings of tyrosine (Tyr), tryptophan (Trp) and phenylalanine (Phe) side chains and vibrations of the sulfur-containing cysteine (Cys) side chain. Many structural correlations have been developed for Raman markers of these side chains and ongoing refinements continue to improve the usefulness of the Raman markers for diagnosis of side chain orientation, interaction or covalency [5–11]. Reviews and critical discussions have been given recently [3,12–14].

In previous work from our laboratories, we reported a combined infrared, Raman and ab initio analysis of the tyrosyl model compound *p*-cresol in the vapor phase [10]. The objectives of that study were to refine earlier vibrational assignments for the *para*-substituted phenolic ring of Tyr [6, 15] and more specifically to identify Raman markers diagnostic of the non-hydrogen-bonded state of the tyrosine phenoxyl group. The latter objective is particularly important for protein applications of Raman spectroscopy because of the well established sensitivity of Raman markers of the tyrosine side chain to the various donor and acceptor roles of the phenoxyl group [6]. The analysis by Arp et al. [10] identified the key Raman markers of tyrosine that were diagnostic of the non-hydrogen-bonded state of the phenolic OH group and demonstrated further that the non-hydrogen-bonded state could account for the unique tyrosyl signatures observed in Raman spectra of capsid protein subunits of filamentous viruses [16,17].

In this work we extend our previous approach to the tryptophan model compound 3-methylindole (3MI) in the vapor phase. 3MI serves as a convenient structural analog of the indolyl side chain of tryptophan (Fig. 1). Raman spectra of 3MI and selected isotopic derivatives were investigated previously to reach reliable assignments for the indolyl moiety, as well as to identify the Raman spectral signature of the tryptophan residue in proteins, and to characterize the dependence of this signature on the local orientation and interactions of the indolyl ring [7,11, 18–21]. The previous studies of the Harada and Takeuchi groups have provided a solid foundation upon which to develop more comprehensive vibrational assignments. Importantly, they facilitate probing the spectral consequences of eliminating (via the gas phase) both the indolyl N1–H donor group and the π-electron acceptor system from participation in significant intermolecular interaction, including hydrogen bonding. The biological significance of the non-hydrogen-bonded state of the tryptophan side chain derives from the frequent occurrence of this residue in the protein subunits of filamentous virus capsids, hydrophobic cores of globular proteins and hydrophobic transmembrane domains of membrane proteins [22]. It is also noteworthy that the π-electron system of the indolyl ring has been implicated as a robust hydrogen-bond acceptor in native proteins [23].

The present results confirm and extend earlier vibrational assignments for the indolyl moiety and demonstrate a remarkable sensitivity of many vibrational bands of the tryptophanyl side chain to intermolecular interaction.

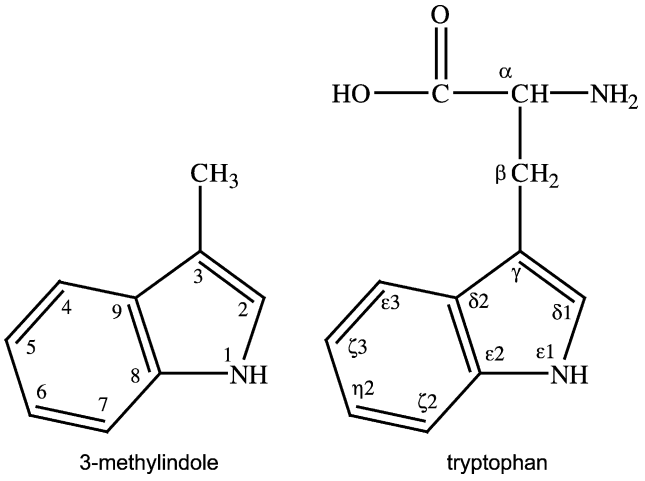

Fig. 1. Structures of 3-methylindole (left) and tryptophan (right). The numbering of ring and exocyclic atoms follows IUPAC-IUPAB nomenclature [31].

2. Materials and methods

3-Methylindole (98%), m.p. 96°, b.p. 266°, was purchased from Aldrich Chemical (St Louis, MO) and purified by trap to trap vacuum distillation. Raman spectra were collected on a Jobin Yvon U-1000 spectrometer (Instruments S. A., Edison, NJ) using excitation at 514.5 nm from an Innova 20 argon-ion laser (Coherent, Santa Clara, CA). The laser power at the sample cell was 2 W for vapor and 800 mW for liquid samples. Vapor phase spectra of approximately 1 atm of sample were obtained at 300 ± 5 °C using a custom-designed thermostatically controlled Raman cell [24] into which solid sample was transferred; the Raman cell was subsequently frozen with liquid nitrogen and sealed after evacuation on a vacuum line. Liquid phase spectra were obtained in a glass tube heated with nichrome wire to 100 °C. Solution spectra at 23 ± 3 °C in various solvents were recorded using quartz cuvettes to contain the samples. Either a charge-coupled device or a photomultiplier tube was used for detection of the Raman scattered light. The Raman spectra were collected and processed using standard software packages (SpectraMax and Bomem Grams).

Infrared spectra were recorded on either a Bomem DA8.02 or a BioRad FTS-60 instrument. Vapor phase spectra at 300 ± 10 °C were recorded using a heatable 10 cm metal cell with KBr windows. Spectra of solid samples (as Nujol mulls) between KBr plates were recorded at 25 °C.

Ab initio calculations were carried out using the GAUSSIAN-03 [25] package at the density functional (B3LYP) level of theory. Structural parameters and vibrational frequencies with infrared and Raman intensities were obtained with the 6-311++G** basis set. Scaling factors of 0.955 for the 2800–3500 cm^{-1} region and 0.985 for the region below 1700 cm^{-1} were used for both our calculations and those of Bunte et al. [26,27].

3. Results

3.1. Experimental and theoretical vibrational spectra of 3-methylindole

Table 1 lists the full Raman (liquid and vapor) and infrared (solid and vapor) spectra of 3-methylindole (3MI) including both unscaled and scaled vibrational frequencies and their approximate vibrational descriptions calculated using the B3LYP/6-311++G** basis set. Fig. 2 compares the experimental Raman spectra of the neat liquid (trace A) and vapor (trace B) with the calculated spectrum (trace C). As in our previous study of *p*-cresol [10], the agreement between observed and calculated values is excellent. The data of Table 1 are also in satisfactory agreement with corresponding data reported by Bunte et al. [26], although some refinements were necessary in the previous assignments and vibrational descriptions, particularly for low frequency modes. We have elected to classify all of the vibrations in accordance with C_S symmetry, so that in-plane and out-of plane vibrations are of species A' and A'', respectively. Because the hydrogen atom at the N^1 indolyl ring site (corresponding to $N^{\varepsilon 1}$ of tryptophan) does not lie precisely in the ring plane, the indole moiety lacks rigorous C_S symmetry. However, this non-planarity has such a small effect that the spectral characteristics are for the most part those of a planar skeleton with C_S symmetry. This is also evident in the work of Bunte et al. [26], i.e. vibrations classified here as A'' are reported by Bunte at al. as depolarized (depolarization ratio $\rho = 0.75$). We have also renumbered the vibrations using the usual convention of high frequencies listed first.

3.2. Ab initio molecular structure of 3-methylindole

The calculated structure of 3MI (6-311++G** basis set) is shown in Fig. 3. The molecular skeleton lies totally within one plane and only the imidazolyl and methyl hydrogens lie outside this plane. The structure shows the expected delocalization of π electrons of the imidazole and phenyl ring systems, which results in a compression of the C^3–C^9 bond of Fig. 1. Other bond lengths and angles are also as expected.

3.3. Raman bands diagnostic of the isolated (non-interacting) 3-methylindole molecule

Evidence for the absence of N^1–H hydrogen bonding by the 3MI molecule in the vapor phase comes from the very high frequency (3506 cm^{-1}) of the Raman band representing the NH stretching mode. The gas-phase 3MI molecule is also presumed to lack other types of intermolecular interactions. Accordingly, the spectrum of trace B in Fig. 2 is considered to represent that of an isolated, non-interacting indolyl moiety.

Comparison of the Raman frequencies and intensities for neat liquid and vapor states of 3MI (Table 1) reveals numerous bands that are strongly sensitive to indolyl intermolecular interactions. For example, ~20 bands exhibit wavenumber shifts of at least 5 cm^{-1}. Of these, four bands are sufficiently intense to be of potential diagnostic value in protein Raman spectra. These are designated as the modes *W*2 [1579 (*l*) and 1585 (*v*) cm^{-1}, for liquid and vapor, respectively], *W*6 [1418 (*l*) and 1409 (*v*) cm^{-1}], *W*7 Fermi pair [1352/1345 (*l*) and 1349/1341 (*v*) cm^{-1}] and *W*17 [875 (*l*) and 881 (*v*) cm^{-1}], in accordance with nomenclature employed previously for protein aromatic ring vibrations [3,28]. In addition, the Fermi doublet intensity ratio (I_1/I_2, where I_1 and I_2 are, respectively, the Raman intensities of the higher and lower wavenumber components of the doublet) is highly sensitive to the state of condensation the 3MI molecule, consistent with the previously reported sensitivity of I_1/I_2 to solvent polarity. We observe $I_1/I_2 = 0.58$ for the liquid and $I_1/I_2 = 3.0$ for the vapor, after deconvolution of the overlapping members of the Fermi pair (Fig. 4).

3.4. Effects of indolyl intermolecular interactions on key Raman markers

The parameter I_1/I_2 of the *W*7 band was also measured for solutions of 3MI in solvents of differing polarity and hydrogen-bonding capability. These measurements complement those of Harada and coworkers [7,11,18–21], who reported effects of solvent polarity on I_1/I_2 and developed several additional structural correlations applicable to spectral parameters of *W*2, *W*6, *W*7 and *W*17. The combined results of this work and previously published data on I_1/I_2 of the *W*7 band are summarized in Table 2. This table also lists the values of the dielectric constants ε_r for the different solvents. Solvents with higher ε_r values are expected to facilitate the intermolecular interactions.

Harada and coworkers proposed that I_1/I_2 is diagnostic of the hydrophobicity of the indolyl ring environment. Specifically, I_1/I_2 increases with increasing hydrophobicity and has been referred to as a 'hydrophobic interaction marker' [11]. This is evident from inspection of Table 2. In addition to *W*7, the sensitivity of the frequencies of the NH stretching and *W*17 modes to indolyl NH hydrogen bonding have been noted [20] and confirmed by the present

Table 1
Experimental and calculated vibrational frequencies of 3-methylindole

Approximate description		Raman		Infrared		Bunte		Ab initio		Bunte ab initio		ρ	
		Liquid	Vapor	Solid	Vapor		Exp.	Unscaled[a]	Scaled	Unscaled	Scaled	ρ	ρ (Bunte)
A′													
1	N–H stretch	3425 m	3506 m	3507/3402 w	3515/3421 vs	51	3493	3678 [532,74]	3512	3682	3516	0.21	0.20
2	=C–H stretch	3119 mw	3118 w	3190 vw	3090 sh w	50	3084	3240 [472,1]	3094	3243	3097	0.31	0.31
3	C–H stretch (Bz)	3058 s	3065 vs	–	3061 vs	49	3060	3189 [1156,18]	3045	3192	3048	0.12	0.13
4	C–H stretch (Bz)	–	3053 sh m	3053 w	3034 vvw	48	3039	3178 [208,30]	3035	3181	3038	0.75	0.75
5	C–H stretch (Bz)	–	–	–	–	47	3017	3167 [540,3]	3025	3171	3028	0.63	0.60
6	C–H stretch (Bz)	–	–	3033 vw	3015 vvw	46	2972	3161 [116,1]	3019	3165	3023	0.70	0.72
7	CH_3 antisym. stretch	2921 ms	2934 s	2931 m	2931 ms	46	2923	3091 [944,22]	2952	3097	2958	0.66	0.66
8	CH_3 sym. stretch	2861 m	2873 m	2858 ms	2870 m	43	2860	3013 [944,50]	2877	3021	2885	0.05	0.03
9	Skeletal stretch (Bz-8b+Pyr)	1618 mw	1620 w	1619 w	1619 w	42	1617	1660 [68,4]	1635	1658	1633	0.74	0.74
10	Skeletal stretch (Bz-8a+Pyr) [*W2*]	1579 ms	1585 sh vw	1589 mw	–	41	1577	1617 [96,0]	1593	1616	1592	0.07	0.05
11	Skeletal stretch (Bz+Pyr)	1559 s	1561 vs	1555 w	1559 w	40	1557	1595 [320,3]	1571	1594	1570	0.26	0.26
12	Skeletal stretch (Bz-19a+Pyr)	1512 vw	–	1486 w	1488 w	39	1493	1522 [10,1.5]	1499	1526	1503	0.68	0.64
13	CH_3 antisym. deformation	1489 w	–	– mw	1472 mw	38	1488	1499 [48,9]	1477	1504	1481	0.67	0.66
14	Skeletal stretch (Bz-19b)/CH wag	1457 m	1454 mw	1455 s	1456 vs	36	1455	1480 [56,26]	1458	1485	1463	0.73	0.71
15	N–H wag [*W6*]	1418 ms	1409 ms	1422 w	1418 m	35	1420	1446 [216,14]	1424	1446	1424	0.53	0.53
16	CH_3 deformation	1384 w	1388/1377 vvw	–	1383	34	1387	1420 [32,1.5]	1399	1424	1403	0.57	0.68
17	Skeletal stretch (Bz-3) [*W7*]	1352/1345 vs	1349/1341 vs	1344 vw	–	33	1345	1373 [240,16]	1352	1372	1351	0.14	0.17
18	Skeletal str (Bz-14+Pyr)/CH/NH wag (Bz+Pyr)	1334 vvw	1324 sh vw	1334 vw	1333 s	32	1334	1365 [44,17]	1345	1366	1346	0.46	0.46
19	Skeletal str (Bz+Pyr)/CH wag (Bz+Pyr)	1299 mw	1292 w	1299 mw	1297 w	31	1302	1319 [44,10]	1300	1322	1302	0.46	0.34
20	CH NH wag (Bz+Pyr)/Ring Bend (Pyr)	1247 m	1245 ms	1247 vw	1247 m	30	1249	1270 [52,11]	1251	1274	1255	0.25	0.16
21	Ring stretch (Pyr)	1227 m	1223 m	1228 w	1225 ms	29	1229	1242 [64,11]	1224	1245	1226	0.13	0.15
22	C–H wag (Bz-15)	1153 w	1142 w	1149 w	1150 vw	28	1149	1176 [4,1]	1159	1180	1162	0.52	0.70
23	C–H wag (Bz-9b)	1126 w	1142 w	1128 mw	1126 vw	27	1126	1148 [12,1]	1131	1150	1133	0.62	0.74
24	=CH NH wag	1085 m	1089 sh vw	1086 ms	1096 sh w	26	1080	1106 [12,26]	1089	1107	1090	0.06	0.13
25	Skeletal deformation/=CH/NH wag	1075 m	1078 m	1069 m	1080 s	25	1070	1090 [40,17]	1074	1091	1075	0.11	0.13
26	Ring breathing (Bz-18b)	1010 vs	1012 vs	1008 m	1010 m	23	1009	1033 [100,11]	1018	1034	1018	0.05	0.04
27	CH_3 rock	980 m	981 m	971 s	980 vvw	21	–	999 [48,6]	984	1001	986	0.07	0.08
28	Skeletal deformation (Bz-12) [*W17*]	875 m	881 ms	898 mw	–	19	876	888 [36,1]	875	891	878	0.08	0.09
29	C–C stretch (Bz)	757 vs	755 vvs	756 m	–	16	758	773 [100,3]	761	774	762	0.05	0.04
30	Ring bend (Bz)	707 m	707 mw	–	–	13	708	718 [28,0.1]	707	719	708	0.21	0.16
31	Skeletal bending	559 m	559 mw	580 ms	–	10	565	570 [32,2]	561	571	562	0.72	0.72
32	Ring bend (Bz)	530 m	530 ms	529 w	–	9	532	539 [24,2]	530	539	531	0.18	0.15
33	Skeletal bending	460 w	463 vvw	497 s	–	8	462	470 [2.4,3]	463	471	464	0.58	0.72
34	CH_3 wag	226 m	228 m	–	–	4	231	225 [8,0.6]	221	224	221	0.63	0.69
A″													
35	CH_3 antisym. stretch	2921 ms	2934 s	2931 m	2931 ms	44	2889	3055 [360,22]	2918	3062	2924	0.75	0.75
36	CH_3 antisym. deformation	1457 m	1454 mw	1455 s	1456 vs	37	1455	1483 [42,7.6]	1461	1486	1464	0.75	0.75
37	CH_3 rock	1065/1026 sh vw	1048 vw	1039 w	–	24	–	1063 [0.12,0.1]	1047	1067	1051	0.75	0.74

38	CH wag (Bz-5)	960 sh vw	963 sh vw	927 m	–	22	983	971 [0.8,0]	956	980	965	0.75	0.75
39	CH wag (Bz)	924 vw	–	900 w	921 w	20	925	934 [1.2,1.4]	855	942	928	0.75	0.75
40	CH wag (Bz)	844 w	842 vw	873/845 w	–	18	–	851 [1.6,0.3]	838	855	842	0.75	0.75
41	=CH wag	799 w	789/807 vvw	804 m	782 w	17	780	792 [12,16]	780	796	784	0.75	0.75
42	Ring twist (Bz)	(757) vs	(755) vvs	(756) vs	–	15	758	772 [0.4,1.2]	760	772	760	0.75	0.68
43	CH wag (Bz-11)	736 w	755	738 vs	736 w	14	731	747 [1.6,88]	736	748	737	0.75	0.75
44	Ring pucker (Pyr)	607 vw	–	605 vw	605 mw	12	601	616 [0.4,0.7]	607	618	609	0.75	0.75
45	Ring twist (Bz-16a)	576 vw	577 sh vw	564 vw	576 w	11	573	585 [0.4,6]	576	590	581	0.75	0.75
46	Benzene oop wag (16a)	426 w	418 vvw	416 s	–	7	426	430 [1.6,4]	423	430	424	0.75	0.75
47	N–H wag	377 vw	–	–	–	6	347	372 [0.8,74]	366	351	346	0.75	0.75
48	Skeletal twist	313 vw	304 vvw	–	–	5	231	284 [2.4,12]	279	248	244	0.75	0.75
49	Skeletal flap	(226) m	–	–	–	3	–	223 [0.2,8]	220	222	219	0.75	0.71
50	CH_3 wag	–	151 m	–	–	2	177	152 [8,5]	150	153	151	0.75	0.75
51	CH_3 torsion	–	–	–	–	1	177	145 [0.8,0.1]	142	137	135	0.75	0.75

Bz, benzene ring vibration; Pyr, pyrrole ring vibration; oop, out of plane; values in brackets also assigned elsewhere; s-strong m-medium w-weak v-very.
[a] Relative Raman and IR intensities, respectively.

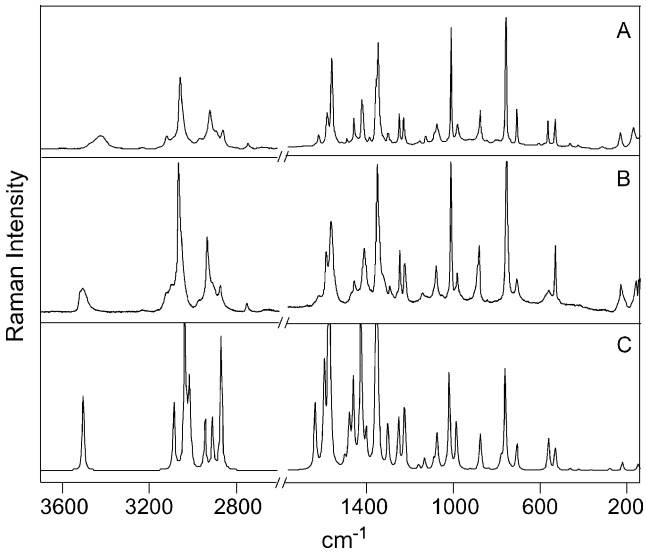

Fig. 2. Raman spectra of 3-methylindole in the region 200–3600 cm^{-1}. (A) Neat liquid (melt at 100 °C). (B) Vapor at 300 °C. (C) Calculated (ab initio) using B3LYP/6-311++G**.

experiments (Fig. 2 and related data not shown). These marker bands are further discussed in the following section.

4. Discussion and conclusions

Miura and coworkers demonstrated that the *W*17 mode of 3MI exhibits an apparent frequency dependence upon the strength of indolyl N–H···O hydrogen bonding [20]. This finding is based upon a close linear correspondence between *W*17 and the frequency of the indolyl NH stretching mode

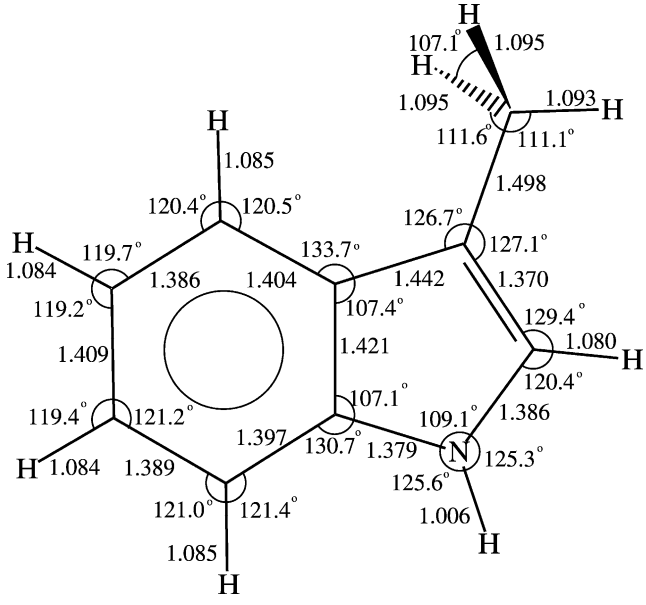

Fig. 3. Calculated molecular structure of 3-methylindole using B3LYP/6-311++G**.

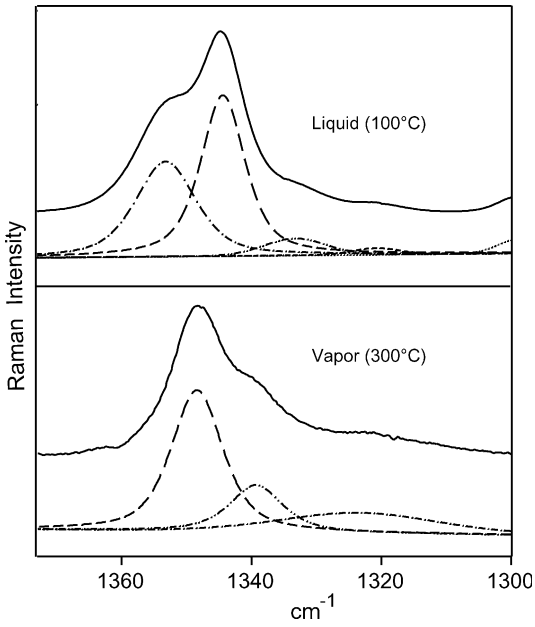

Fig. 4. Raman spectra of 3-methylindole in the region 1300–1375 cm^{-1} showing the Fermi doublet (mode *W*7). Experimental data (solid line) and curve fits of the deconvolved data for the neat liquid at 100 °C and vapor at 300 °C are shown in the top and bottom panels, respectively. Data are from Fig. 2A and B.

when the hydrogen bonding environment of 3MI is varied. Raman and infrared spectral data collected from solutions of 3MI in solvents of diverse O-acceptor capabilities and from crystals of indolyl model compounds of known X-ray structure provide the experimental support [20]. The proposed structural correlation has been exploited recently to characterize tryptophan hydrogen bonding interactions in native proteins [7,29,30]. A keystone of the structural correlation is the observation that in a non-hydrogen-bonding solvent, such as CS_2 ($\varepsilon_r = 2.24$) or cyclohexane ($\varepsilon_r = 2.02$), the NH stretching and *W*17 modes occur near 3476 (infrared) and 883 (Raman) cm^{-1}, respectively [20]. However, Raman frequencies of 3MI in the prototypical non-hydrogen-bonded state—viz the vapor—were not reported previously.

In the present work we have determined that the NH stretching and *W*17 modes of 3MI vapor occur at 3506 and 881 cm^{-1}, respectively, which constitute a data point only slightly deviant from the previously proposed linear relationship of Miura et al. (Fig. 2 of Ref. [20]). Accordingly, our results are consistent with the proposition that the wavenumber value of the *W*17 mode is a reliable indicator of indolyl N^1–H hydrogen bond donation. Specifically, we conclude that the non-hydrogen-bonded N–H group exhibits *W*17 at 882 ± 1 cm^{-1}, while the very strongly hydrogen bonded N–H group exhibits *W*17 at 871 ± 1 cm^{-1}. The former state is represented by the vapor (this work) and both CS_2 and cyclohexane solutions of 3MI [20], while the latter is represented by the N–H···O bond in the crystal structure of *N*-acetyl-DL-tryptophan methylamide [20].

With respect to the relative Raman intensity ratio (I_1/I_2) of the components of the Fermi doublet (*W*7), the situation appears to be more complex (Table 2). Our underlying hypothesis is again that the 3MI molecule in the vapor is devoid of any intermolecular interactions. Accordingly, in the absence of intermolecular contacts with either

Table 2
Raman solution spectra frequencies of the *W*7 band

Phase	Concentration (mM)	Raman frequency (cm^{-1})		Ratio (I_1/I_2)[a]	Dielectric constant[b]	Reference
Vapor	–	1349	1341	3.0	–	[c]
Solvent						
Cyclohexane	100	1352	1343	1.55	2.02	[c]
n-Hexane	100–200	1352	1343	1.50	1.89	[18]
Carbon disulfide	100–200	1350	1341	1.18	2.24	[18]
Methanol-d	500	1353	1346	1.18	–	[c]
Methanol-d	100	1354	1346	1.06	–	[c]
Toluene	100–200	1341	1343	1.04	2.38	[18]
Carbon tetrachloride	100	1353	1344	0.99	2.24	[c]
Benzene	100–200	1351	1343	0.96	2.28	[18]
Benzene	100	1353	1344	0.89	2.28	[c]
Benzene	500	1353	1344	0.83	2.28	[c]
o-Dichlorobenzene	100–200	1351	1343	0.83	10.12	[18]
Tetrahydrofuran	100	1354	1346	0.71	7.52	[c]
Methanol	100	1353	1346	0.48	33.0	[c]
Methanol	300	1355	1346	0.45	33.0	[c]
Chloroform	100	1354	1345	0.43	4.81	[c]
Neat Liquid(melt)	–	1352	1345	0.58	–	[c]

[a] (I_1/I_2) is the intensity ratio of the higher frequency band to the lower frequency band.
[b] CRC Handbook of Chemistry and Physics, 85th ed., pp. 8–141.
[c] Data from this work.

hydrophobic or polar molecules, including potential hydrogen bonding partners for the exocyclic (N^1–H) or aromatic (π-electron) groups of 3MI, I_1/I_2 achieves its maximum value of 3.0. This value falls sharply with the introduction of any intermolecular environment represented by the solvents of Table 2. For non-polar and non-hydrogen-bonding solvent environments the range observed is $0.8 < I_1/I_2 < 1.6$, which is twofold to threefold lower than the maximum observed for the vapor. In the case of polar and hydrogen bonding solvent environments, I_1/I_2 is further diminished by another factor of two, i.e. $0.4 < I_1/I_2 < 0.8$. Therefore, the I_1/I_2 ratio is strongly sensitive to factors other than simply NH or π hydrogen bonding, namely to the intermolecular environment of the indolyl ring and the relative hydrophobicity/hydrophilicity of that environment.

Our results show that the strength of Fermi coupling of *W7* is relatively weak for the noninteracting indolyl ring (vapor phase). This results in a relatively large intensity imbalance ($I_1/I_2 \sim 3.0$) between the two components of the Fermi doublet. Upon introducing interactions with hydrophobic molecular neighbors (apolar solvents), the Fermi coupling is strengthened and the doublet components approach parity of intensity ($I_1/I_2 \sim 1$). Further, as the hydrophobicity of the local indolyl ring environment is diminished in favor of hydrophilicity (polar solvents), the strength of Fermi coupling again weakens and the parity of intensity of the doublet components is diminished ($I_1/I_2 \sim 0.4$).

Takeuchi and co-workers [11] have attributed the Fermi coupling to resonance between the *W7* in-plane fundamental vibration (mainly $N^1{=}C^8$ bond stretching) and one or more combination bands due to out-of-plane vibrations. These authors speculate that small changes in the hydrophobic character of the solvent could affect the frequencies of the out-of-plane components and impact the strength of Fermi coupling. While this may explain the solution results, it does not explain the persistence of Fermi coupling in the vapor phase spectrum of 3MI. The present results show that even in the absence of solvent interactions at the faces of the indolyl plane, Fermi coupling is sufficient to generate a recognizable doublet in the Raman spectrum.

The complexity of Fermi coupling in the 1330–1370 cm^{-1} region of the indole Raman signature is further complicated by recent data obtained on bacteriorhodopsin [30]. A tryptophan residue of this protein generates an apparent *W7* triplet (1370/1357/1339 cm^{-1}) in lieu of the doublet normally encountered in protein Raman and UVRR spectra. These results suggest the need for additional studies to elucidate the origins of *W7* Fermi coupling and factors affecting the intensities of the multiplet components.

Acknowledgements

This paper is most appropriate for this journal issue published in honor of Professor Hiroaki Takahashi as he is a good friend of both principal investigators (JL and GT). Moreover, this work is a follow-up of studies initiated by the late Professor Issei Harada, who was a very good friend of all three of us. JL thanks the National Science Foundation (Grant CHE-0131935) and the Robert A. Welch Foundation (Grant A-0396) for support. GT thanks the National Institutes of Health (Grant GM 50776) for support. DA gratefully acknowledges summer support from the FSU-RISE grant funded by the National Institutes of Health, Grant 1R25GM64508.

References

[1] M. Berjot, J. Marx, A.J.P. Alix, J. Raman Spectr. 18 (1987) 289–300.
[2] J. Bandekar, Biochim. Biophys. Acta 1120 (1992) 123–143.
[3] J.C. Austin, T. Jordan, T.G. Spiro, Ultraviolet resonance Raman studies of proteins and related compounds in: R.J.H. Clark, R.E. Hester (Eds.), Biomolecular Spectroscopy, Part A, Wiley, New York, 1993, pp. 55–127.
[4] S.U. Sane, S.M. Cramer, T.M. Przybycien, Anal. Biochem. 269 (1999) 255–272.
[5] R.C. Lord, N.T. Yu, J. Mol. Biol. 50 (1970) 509–524.
[6] M.N. Siamwiza, R.C. Lord, M.C. Chen, T. Takamatsu, I. Harada, H. Matsuura, T. Shimanouchi, Biochemistry 14 (1975) 4870–4876.
[7] T. Miura, H. Takeuchi, I. Harada, Biochemistry 30 (1991) 6074–6080.
[8] H. Li, G.J. Thomas Jr, J. Am. Chem. Soc. 113 (1991) 456–462.
[9] S.W. Raso, P.L. Clark, C. Haase-Pettingell, J. King, G.J. Thomas Jr, J. Mol. Biol. 307 (2001) 899–911.
[10] Z. Arp, D. Autrey, J. Laane, S.A. Overman, G.J. Thomas Jr, Biochemistry 40 (2001) 2522–2529.
[11] H. Takeuchi, Biopolymers 72 (2003) 305–317.
[12] T. Miura, G.J. Thomas Jr, Subcell. Biochem. 24 (1995) 55–99.
[13] G.J. Thomas Jr, Biopolymers 67 (2002) 214–225.
[14] J.M. Benevides, S.A. Overman, G.J. Thomas Jr, Raman spectroscopy of proteins in: J.E. Coligan, B.M. Dunn, H.L. Ploegh, D.W. Speicher, P.T. Wingfield (Eds.), Current Protocols in Protein Science (2003), pp. 17.8.1–17.8.35.
[15] H. Takeuchi, N. Watanabe, I. Harada, Spectrochim. Acta 44A (1988) 749–761.
[16] S.A. Overman, K.L. Aubrey, N.S. Vispo, G. Cesareni, G.J. Thomas Jr, Biochemistry 33 (1994) 1037–1042.
[17] S.A. Overman, G.J. Thomas Jr, Biochemistry 34 (1995) 5440–5451.
[18] I. Harada, T. Miura, H. Takeuchi, Spectrochim. Acta 42A (1986) 307–312.
[19] H. Takeuchi, H. Harada, Spectrochim. Acta 42A (1986) 1069–1078.
[20] T. Miura, H. Takeuchi, I. Harada, Biochemistry 27 (1988) 88–94.
[21] T. Miura, H. Takeuchi, I. Harada, J. Raman Spectrosc. 20 (1989) 667–671.
[22] S.K. Burley, G.A. Petsko, Adv. Protein Chem. 39 (1988) 125–189.
[23] J.P. Gallivan, D.A. Dougherty, Proc. Natl. Acad. Sci. USA 96 (1999) 9459–9464.
[24] J. Laane, K. Haller, S. Sakuri, M. Morris, D. Autrey, Z. Arp, W. Chiang, A. Combs, J. Mol. Struct. 650 (2003) 57–68.
[25] GAUSSIAN-03, Revision C.02, M.J. Frisch, G.W. Trucks, H.B. Schlegel, G.E. Scuseria, M.A. Robb, J.R. Cheeseman, J.A. Montgomery, Jr., T. Vreven, K.N. Kudin, J.C. Burant, J.M. Millam, S.S. Iyengar, J. Tomasi, V. Barone, B. Mennucci, M. Cossi, G. Scalmani, N. Rega, G.A. Petersson, H. Nakatsuji, M. Hada, M. Ehara, K. Toyota, R. Fukuda, J. Hasegawa, M. Ishida, T. Nakajima, Y. Honda, O. Kitao, H. Nakai, M. Klene, X. Li, J.E. Knox, H.P. Hratchian, J.B. Cross, C. Adamo, J. Jaramillo, R. Gomperts, R.E. Stratmann, O. Yazyev, A.J. Austin, R. Cammi, C. Pomelli, J.W. Ochterski, P.Y. Ayala, K. Morokuma, G.A. Voth, P. Salvador, J.J. Dannenberg, V.G.

Zakrzewski, S. Dapprich, A.D. Daniels, M.C. Strain, O. Farkas, D.K. Malick, A.D. Rabuck, K. Raghavachari, J.B. Foresman, J.V. Ortiz, Q. Cui, A.G. Baboul, S. Clifford, J. Cioslowski, B.B. Stefanov, G. Liu, A. Liashenko, P. Piskorz, I. Komaromi, R.L. Martin, D.J. Fox, T. Keith, M.A. Al-Laham, C.Y. Peng, A. Nanayakkara, M. Challacombe, P.M.W. Gill, B. Johnson, W. Chen, M.W. Wong, C. Gonzalez, and J.A. Pople, Gaussian, Inc., Wallingford CT, 2004.

[26] S. Bunte, G. Jensen, K. McNesby, D. Goodin, C. Chabalowski, R. Nieminen, S. Suhai, K. Jalkanen, Chem. Phys. 265 (2001) 13–25.

[27] G. Jensen, D. Goodin, S. Bunte, J. Phys. Chem. 100 (1996) 954–959.

[28] T.G. Spiro, Biological Applications of Raman Spectroscopy, Raman Spectra and the Conformations of Biological Macromolecules, vol. 1, Wiley, New York, 1987.

[29] S. Hashimoto, K. Obata, H. Takeuchi, R. Needleman, J.K. Lanyi, Biochemistry 36 (1997) 11583–11590.

[30] S. Hashimoto, M. Sasaki, H. Takeuchi, R. Needleman, J.K. Lanyi, Biochemistry 41 (2002) 6495–6503.

[31] J.L. Markley, A. Bax, Y. Arata, C.W. Hilbers, R. Kaptein, B.D. Sykes, P.E. Wright, K. Wuthrich, J. Mol. Biol. 280 (1998) 933–952.